

# Reversible electron beam heating for suppression of microbunching instabilities at free-electron lasers

Christopher Behrens<sup>1</sup>, Zhirong Huang<sup>2</sup>, and Dao Xiang<sup>2</sup>

<sup>1</sup> *Deutsches Elektronen-Synchrotron DESY, Notkestr. 85, 22607 Hamburg, Germany*

<sup>2</sup> *SLAC National Accelerator Laboratory, Menlo Park, CA 94025, USA*

(Dated: May 3, 2022)

The presence of microbunching instabilities due to the compression of high-brightness electron beams at existing and future X-ray free-electron lasers (FELs) results in restrictions on the attainable lasing performance and renders beam imaging with optical transition radiation impossible. The instability can be suppressed by introducing additional energy spread, i.e., “heating” the electron beam, as demonstrated by the successful operation of the laser heater system at the Linac Coherent Light Source. The increased energy spread is typically tolerable for self-amplified spontaneous emission FELs but limits the effectiveness of advanced FEL schemes such as seeding. In this paper, we present a reversible electron beam heating system based on two transverse deflecting radio-frequency structures (TDSs) in front and behind a magnetic bunch compressor chicane. The additional energy spread will be introduced in the first TDS, which suppresses the microbunching instability, and then will be eliminated in the second TDS. We show the feasibility of the microbunching gain suppression based on calculations and simulations including the effects of coherent synchrotron radiation. Acceptable electron beam and radio-frequency jitter will be identified, and options for integrated diagnostics and on-line monitoring of the electron beam’s longitudinal phase space will be discussed.

PACS numbers: 29.27.-a, 41.60.Cr, 41.85.Ct

## I. INTRODUCTION

X-ray free-electron lasers (FELs) provide an outstanding tool for studying matter at ultrafast time and atomic length scales [1], and have become a reality with the operation of the Free-electron Laser in Hamburg (FLASH) [2], the Linac Coherent Light Source (LCLS) [3], and the SPring-8 Angstrom Compact Free Electron Laser (SACLA) [4]. The required high transverse and longitudinal brightness of the X-ray FEL driving electron bunches may encounter various degradation effects due to collective effects like coherent synchrotron radiation (CSR) or microbunching instabilities (e.g., Refs. [5–7]), and need to be preserved and controlled. In order to suppress a microbunching instability associated with longitudinal bunch compression that deteriorates the FEL performance, LCLS uses a laser heater system to irreversibly increase the slice energy spread to a level tolerable for operation of a self-amplified spontaneous emission FEL [8, 9]. For future X-ray FELs that plan to use external lasers to seed the FEL process in order to achieve better temporal coherence and synchronization for pump-probe experiments, a smaller slice energy spread is required to leave room for the additional energy modulation imprinted by the seed laser. Thus, the amount of tolerable heating is more restrictive and the longitudinal phase space control becomes more critical (e.g., Refs. [10, 11]). The same strict requirement on small slice energy spreads is valid for optical klystron enhanced self-amplified spontaneous emission free-electron lasers [12].

Originally designed for particle separation by radio-frequency (rf) fields [13], transverse deflecting rf structures (TDSs) are routinely used for high-resolution tem-

poral diagnostics in X-ray FELs (e.g., Refs. [14–17]) and are proposed to use for novel beam manipulation methods (e.g., Refs. [18–23]). Recently, a TDS was used to increase the slice energy spread in an echo-enabled harmonic generation experiment [24, 25]. In this paper, we present a reversible electron beam heating system that uses two TDSs located in front and behind a magnetic bunch compressor chicane. The additional energy spread will be introduced in the first TDS, which suppresses the microbunching instability, and then will be eliminated in the second TDS.

The method of reversible beam heating will be shown in Sec. II by means of linear beam optics and a corresponding matrix formalism. In Sec. III, we show the feasibility of this scheme to preserve both the transverse and longitudinal brightness of the electron beam and discuss the impact of coherent synchrotron radiation. Section IV covers the gain suppression of microbunching instabilities by analytical calculations and numerical simulations, and in Sec. V, we discuss the impact of beam and rf jitter and show inherent options for diagnosis and on-line monitoring of the electron beam’s longitudinal phase space. The results and conclusions are summarized in Sec. VI.

## II. METHOD

In this and the following sections, we consider a linear accelerator (linac) employing a single bunch compressor for a soft X-ray FEL, such as the proposed linac configuration for the Next Generation Light Source (NGLS) at LBNL [26]. The choice of a single bunch compressor simplifies our consideration and analysis, although the concept is applicable for typical bunch compressor ar-

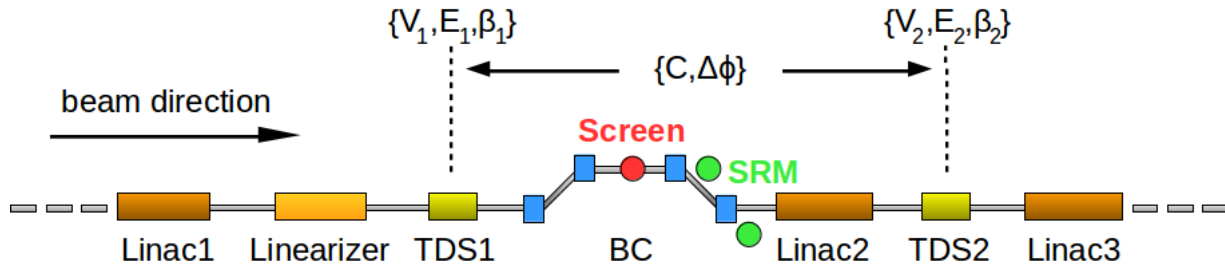


FIG. 1: Layout of an reversible electron beam heater system including two transverse deflecting rf structures located in front and behind a magnetic bunch compressor (BC) chicane and integrated longitudinal phase space diagnostics using screens and synchrotron radiation monitors (SRM). Parameters related to the reversible beam heater system are denoted in curly brackets.

rangements with multiple stages. We note that a single bunch compressor arrangement has also been considered for the FERMI@Elettra FEL to minimize the impact of microbunching instabilities [27].

The generic layout of an reversible electron beam heater system is depicted in Fig. 1. It consists of linac sections providing and accelerating high-brightness electron beams, a magnetic bunch compressor chicane in order to achieve sufficient peak currents to drive the FEL process, and two transverse deflecting rf structures located in front and behind the bunch compressor. An additional higher-harmonic rf linearizer system (Linearizer), like at LCLS or FLASH [28], can be used to achieve uniform compression by means of longitudinal phase space linearization in front of the bunch compressor (see Appendix for details). The whole system can be supplemented by dedicated longitudinal phase space diagnostics (will be discussed in Sec. V), and except for the two TDSs, the layout is commonly used for bunch compression at present and future X-ray FELs.

The principle of the reversible electron beam heater relies on the physics of TDSs arising from the Panofsky-Wenzel theorem [29]

$$\Delta \vec{p}_\perp = -i \frac{e}{\omega} \int_0^L \nabla_\perp \mathcal{E}_z dz, \quad (1)$$

where  $\omega/(2\pi)$  is the operating rf frequency,  $e$  is the elementary charge, and  $L$  is the structure length. The theorem states that the transverse momentum gain of an electron imprinted by a TDS is related to the transverse gradient of the longitudinal electric field. Operating a TDS (throughout this paper, we assume vertical deflection, i.e., in  $y$ -direction) near the zero-crossing rf phase, electrons experience transverse kicks [14]

$$\Delta y' = \frac{e\omega V_y}{cE} z_i = K_y z_i \quad (2)$$

and relative energy gains ( $\delta = \Delta E/E$ ) [30, 31]

$$\Delta \delta = K_y \frac{1}{L} \int_0^L y(s) ds = K_y \bar{y}, \quad (3)$$

where  $K_y = e\omega V_y/(cE)$  is the vertical kick strength,  $V_y$  is the peak deflection voltage in the TDS,  $c$  is the speed of light in vacuum,  $E$  is the electron energy,  $z_i$  is the initial longitudinal position of the electron relative to the zero-crossing rf phase, and  $\bar{y}$  is the mean vertical position relative to the optical axis inside the finite TDS. Both the additional transverse kicks and relative energy gains are induced by the TDS operation itself and show intrinsic correlations which will also be present in a system of many electrons, i.e., in an electron bunch. In fact, the induced transverse kick correlates linearly with the internal longitudinal bunch coordinate  $z = t/c$  and enables high-resolution temporal diagnostics (e.g., Refs. [14–16]), whereas the induced relative energy gain correlates with the vertical position inside the TDS and results in an induced relative energy spread  $\Delta \sigma_\delta = K_y \sigma_{y_i}$ . This additional energy spread (cf. laser heater [8, 9]), in combination with the momentum compaction  $R_{56}$  of a bunch compressor chicane, is able to smear microbunch structures and correspondingly suppresses the associated instability as shown in Sec. IV. The effect of induced energy spread (“beam heating”) is generated by off-axis longitudinal electric fields, related to the principle of a TDS by the Panofsky-Wenzel theorem, and has been observed experimentally at FLASH [32] and LCLS [33]. The induced energy spread is uncorrelated in the longitudinal phase space ( $z, \delta$ ), but shows correlations in the phase space ( $y, \delta$ ) which is the reason that it can be eliminated (“beam cooling”) with a second TDS in a reversible mode as shown in the following by two different approaches.

### A. Linear beam optics

The transverse betatron motion of an electron passing through a TDS with vertical deflection is given by (e.g., Refs. [14, 15, 31])

$$y(s) = y_0(s) + S_y(s, s_0) z \quad (4)$$

with the vertical shear function

$$S_y(s, s_0) = M_y^{1,2} K_y = \sqrt{\beta_y(s)\beta_y(s_0)} \sin(\Delta\phi_y) \frac{e\omega V_y}{cE}, \quad (5)$$

where  $M_y^{1,2} = \sqrt{\beta_y(s)\beta_y(s_0)} \sin(\Delta\phi_y)$  is the angular-to-spatial element of the vertical beam transfer matrix from the TDS at  $s_0$  to any position  $s$ ,  $\beta_y$  is the vertical beta function,  $\Delta\phi_y$  is the vertical phase advance between  $s_0$  and  $s$ , and  $y_0(s)$  describes the intrinsic motion independent of any TDS shearing effect. Referring to the layout depicted in Fig. 1 and taking bunch compression into account, the entire vertical betatron motion behind the second TDS becomes (omitting the index  $y$  and argument  $s$  in the following, e.g.  $S_1$  instead of  $S_{y,1}(s)$ )

$$y = y_0 + S_1 z_1 + S_2 z_2 = y_0 + (CS_1 + S_2) z_2 \quad (6)$$

with the compression factor  $C = z_1/z_2$  and the shear functions  $S_1$  and  $S_2$  of the corresponding TDSs. Here,  $y_0 + S_1 z_1$  is the TDS2-independent motion like  $y_0(s)$  in Eq. (4). In order to cancel the spatial chirp induced by the combined TDS operation, the  $z$ -dependent term ( $CS_1 + S_2$ ) must vanish. Using Eq. (5) and taking acceleration in Linac2 into account by  $\beta_1 \beta_f \rightarrow \beta_1 \beta_f E_1/E_2$  [14], we get

$$C\sqrt{\beta_1} \sin(\Delta\phi_{1f}) \sqrt{\frac{E_1}{E_2}} K_1 + \sqrt{\beta_2} \sin(\Delta\phi_{2f}) K_2 = 0, \quad (7)$$

where the indices 1, 2 and  $f$  denote the positions, e.g.,  $\Delta\phi_{1f}$  is the vertical phase advance from the first TDS at position  $s_1$  to any position  $s_f$  and  $\Delta\phi_{12} = \Delta\phi_{1f} - \Delta\phi_{2f}$  is the phase advance between the TDSs. A general solution, valid for any position  $s_f$  behind the second TDS, is only possible for a phase advance of

$$\Delta\phi_{12} = n \cdot \pi \quad (8)$$

with  $n$  being integer, and the kick strength

$$K_2 = \pm C \sqrt{\frac{\beta_1}{\beta_2}} \sqrt{\frac{E_1}{E_2}} K_1, \quad (9)$$

where the sign depends on the actual phase advance, i.e.,  $\Delta\phi_{12} = \pi + n \cdot 2\pi$  for (+) and  $\Delta\phi_{12} = n \cdot 2\pi$  for (-). The different sign of  $K$  can technically be achieved by changing the rf phase in the TDS by  $180^\circ$  which results in a zero-crossing rf phase with opposite slope and deflection. Besides cancelation of the induced spatial chirps, the induced energy spread of the first TDS needs to be eliminated in the second structure in order to have a fully reversible electron beam heater. Applying Eq. (3) similar to Eq. (6), the relative energy deviation behind the second TDS becomes

$$\delta = (\delta_0 + K_1 \bar{y}_1) C \frac{E_1}{E_2} + K_2 \overline{(y_2 + S_1 z_1)} \quad (10)$$

with the intrinsic relative energy deviation  $\delta_0$  and the mean positions  $\bar{y}_1$  and  $\bar{y}_2$  inside the TDSs. The second

term involves the spatial chirp induced by the first TDS with  $S_1 \sim \sin(\Delta\phi_{12})$ , and vanishes in the case of spatial chirp cancelation given by Eq. (8). In order to cancel the relative energy spread induced by the combined TDS operation, it follows

$$K_1 \bar{y}_1 C \frac{E_1}{E_2} + K_2 \bar{y}_2 = 0. \quad (11)$$

The beam transport optics for the phase advance condition in Eq. (8) gives  $\bar{y}_2 = \pm \bar{y}_1 \sqrt{\beta_2/\beta_1}$ , and taking  $\beta_2 \rightarrow \beta_2 E_1/E_2$  (see prior Eq. (7)) into account yields exactly the same condition as in Eq. (9). Simultaneous spatial chirp and energy spread cancelation in the second TDS is the basic principle for reversible electron beam heating and enables local increase of energy spread, e.g., exclusively in a bunch compressor. The amount of additional energy spread can be controlled by the kick strength  $K_1$  and the vertical beam size  $\sigma_{y,1}$ .

In the following, a complementary approach to discuss the reversible heating system will be shown. It will use the matrix formalism for beam transport and provides an analytical way to show microbunching gain suppression and to discuss the impact of beam and rf jitter.

## B. Matrix formalism

We adopt the transport matrix notation of a 6x6 matrix for  $(x, x', y, y', z, \delta)$  but leaves  $(x, x')$  out for simplicity, i.e.,  $(y, y', z, \delta)$  will be used in the following. The 4x4 transport matrix for a TDS (with deflection in  $y$ -direction) in thin-lens approximation is given by (e.g., Refs. [19, 30, 32])

$$\mathbf{R}_T^{thin} = \begin{pmatrix} 1 & 0 & 0 & 0 \\ 0 & 1 & K & 0 \\ 0 & 0 & 1 & 0 \\ K & 0 & 0 & 1 \end{pmatrix}. \quad (12)$$

As discussed above, the main components of the given reversible heater system shown in Fig. 1 consists of TDS1 with the kick strength  $K_1$ , a bunch compressor with the momentum compaction factor  $R_{56}$ , and TDS2 with the kick strength  $K_2$ . Including the momentum compaction from the bunch compressor, the 4x4 matrix between two TDSs can be written as

$$\mathbf{R}_C = \begin{pmatrix} a & b & 0 & 0 \\ c & d & 0 & 0 \\ 0 & 0 & 1 & R_{56} \\ 0 & 0 & 0 & 1 \end{pmatrix}. \quad (13)$$

In order to allow the energy change in the first TDS to be compensated for in the second TDS, we require  $b = 0$ , corresponding to an equivalent vertical phase advance of  $\Delta\phi = n \cdot \pi$  with  $n$  being integer (see Eq. (8)). Then we get the magnification factor  $a = \pm \sqrt{\beta_2/\beta_1}$  and  $d = 1/a$ .

The linear accelerator section with higher-harmonic rf linearizer (Linac1 and Linearizer) in front of the first

transverse deflecting rf structure will introduce an appropriate energy chirp  $h$  for uniform bunch compression (see Appendix for details), and the linac section behind the bunch compressor (Linac2/3) will impose an opposite energy chirp  $-h/(1+hR_{56})$  to cancel the residual energy chirp. Without loss of generality, we neglect acceleration between the two TDSs, i.e., we do not consider Linac2 anymore. Including Linac2 would simply result in a correction term  $\sqrt{E_1/E_2}$  (cf. Eqs. (9) and (15) below) but would leave the physics unchanged. The entire beam transport matrix becomes

$$\begin{pmatrix} a & 0 & 0 & 0 \\ c + K_1 K_2 R_{56} & \frac{1}{a} & \frac{K_1}{a} + K_2(1+hR_{56}) & K_2 R_{56} \\ K_1 R_{56} & 0 & 1+hR_{56} & R_{56} \\ \frac{K_1}{1+hR_{56}} + aK_2 & 0 & 0 & \frac{1}{1+hR_{56}} \end{pmatrix}. \quad (14)$$

Cancellation of induced spatial chirps and relative energy spread require  $R_{45} = R_{63} = 0$  (6x6-matrix notation), i.e.,

$$K_1/a + K_2(1+hR_{56}) = 0. \quad (15)$$

For uniform compression with  $C^{-1} = (1+hR_{56})$ , no acceleration in Linac2, i.e.,  $E_1 = E_2$ , and taking into account that  $a = \pm\sqrt{\beta_2/\beta_1}$ , this expression is identical to Eq. (9) and both formalisms show the same result.

Since the kick strength of the first TDS is very weak, it can be implemented by means of a short rf structure and the thin-lens approximation is still valid. However, the kick strength of the second TDS is usually stronger, and the effect of the finite structure length should be taken into account. The symplectic matrix of a thick TDS with the length  $L_2$  is given in Ref. [19] by

$$\mathbf{R}_T^{thick} = \begin{pmatrix} 1 & L_2 & K_2 L_2/2 & 0 \\ 0 & 1 & K_2 & 0 \\ 0 & 0 & 1 & 0 \\ K_2 & K_2 L_2/2 & K_2^2 L_2/6 & 1 \end{pmatrix}. \quad (16)$$

In this case, we should make sure the point-to-point imaging is from the first TDS to the middle of the second TDS ( $b = -dL_2/2$  in Eq. (13)), and adjust the Linac3 chirp to also cancel the induced energy chirp ( $R_{65} = 0$  in 6x6-matrix notation) of the second TDS. After the straightforward matrix multiplication, the overall matrix after Linac3, when Eq. (15) is fulfilled, becomes

$$\begin{pmatrix} \frac{2}{d} - a + \frac{K_1 K_2 R_{56} L_2}{2} & \frac{dL_2}{2} & 0 & \frac{K_2 L_2 R_{56}}{2} \\ c + K_1 K_2 R_{56} & d & 0 & K_2 R_{56} \\ K_1 R_{56} & 0 & 1+hR_{56} & R_{56} \\ 0 & 0 & 0 & \frac{1}{1+hR_{56}} \end{pmatrix}. \quad (17)$$

Here, a few correction terms containing the length  $L_2$  of the second TDS appear, which however does not change the working principle of the reversible heater system. It should be pointed out that behind the reversible heater system, the beam is slightly coupled in  $y' - \delta$  and  $y - z$ , which results in a small growth in projected emittance,

$$\epsilon_{y,z}^2 = \epsilon_{y0,z0}^2 + \epsilon_{y0}\epsilon_{z0} \frac{\beta_{y0}\gamma_{z0}K_1^2 R_{56}^2}{(1+hR_{56})^2} \quad (18)$$

where  $\epsilon_{y0,z0}$  is the initial vertical (longitudinal) emittance,  $\beta_{y0}$  and  $\gamma_{z0}$  are the initial Twiss parameters. As will be shown in the following section, this emittance growth is typically negligible.

### III. REVERSIBLE HEATING AND EMITTANCE PRESERVATION

We demonstrate the feasibility of the reversible beam heater system by numerical simulations using the particle tracking code *legant* [34]. If not specified, the simulations in the following include  $5 \times 10^5$  particles. Table I summarizes the main parameters used in the simulations, and the adopted accelerator optics model, including the positions of the TDSs, is shown in Fig. 2. Except for the TDSs, the parameters are similar to the magnetic bunch compressor system discussed for the Next Generation Light Source at LBNL [26, 35].

TABLE I: Parameters of the electron beam, the bunch compressor system, and of the transverse deflecting rf structures.

Parameter	Symbol	Value	Unit
Beam energy in TDS1/2	$E$	350	MeV
Initial transverse emittance	$\gamma\epsilon_{x,y}$	0.6	$\mu\text{m}$
Initial slice energy spread	$\sigma_E$	$\sim 1$	keV
Momentum compaction factor	$R_{56}$	-138	mm
Compression factor	$C$	$\sim 13$	
Final bunch current	$I_f$	$\sim 520$	A
TDS1/2 rf frequency	$\omega/2\pi$	3.9	GHz
Voltage of TDS1	$V_1$	0.415	MV
Voltage of TDS2 (without CSR)	$V_2$	5.440	MV
Length of TDS1	$L_1$	0.1	m
Length of TDS2	$L_2$	0.5	m

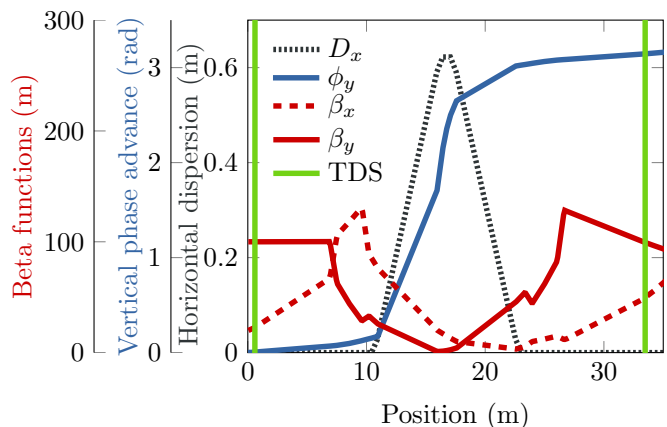


FIG. 2: Relevant accelerator optics (Twiss parameters) and positions of the transverse deflecting rf structures used to numerically demonstrate the reversible beam heater system.

The initial electron bunch is assumed to be flat-top

with a peak current of  $\sim 40$  A and a slice energy spread of  $\sim 1$  keV (r.m.s.). The initial linear and quadratic chirp is set for a uniform bunch length. This is possible even with bunch compressor chicane nonlinearities, i.e.,  $T_{566}$ , by using a higher-harmonic rf linearizer in front of the bunch compressor (see Appendix for details).

Figure 3 shows the principle of the reversible beam heater system, by means of simulation of the longitudinal phase space at different locations along the beam-line. The impact of CSR is not taken into account (cf.

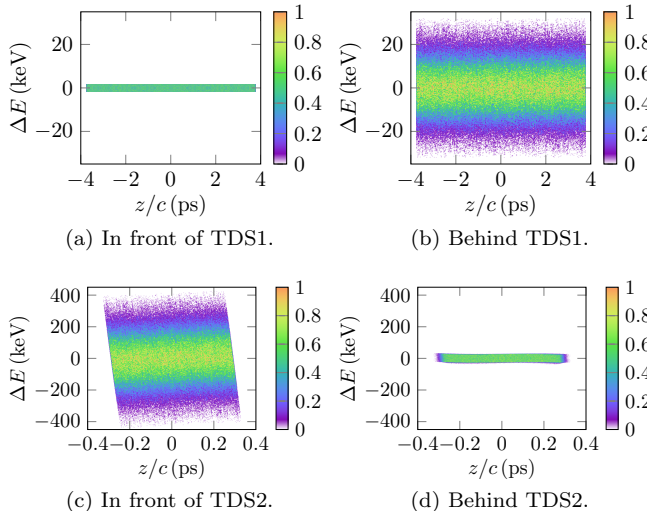


FIG. 3: Simulation of the longitudinal phase space: (a) in front of the first TDS, (b) directly behind the first TDS, (c) directly behind the bunch compressor and in front of the second TDS, and (d) behind the second TDS. The axes scales change from (b) to (c) when bunch compression takes place.

next subsection for CSR effects). The initial slice energy spread is heated up in the first TDS to  $\sim 10$  keV (Fig. 3(b)), increased by the compression factor in the bunch compressor to  $\sim 130$  keV (Fig. 3(c)), and finally cooled down by the second TDS to  $\sim 13$  keV (Fig. 3(d)). The plot in Fig. 4(b) shows that the heating induced by the first TDS is perfectly reversible and the final slice energy spread is simply the initial slice energy spread scaled with the compression factor, which would be exactly the same like in the case without using the reversible beam heater system. Figure 4(a) shows the heater system impact on both the projected emittance (horizontal and vertical) and the core energy spread, i.e., the slice energy spread in the center of the bunch, for different voltages in the second TDS. The minimum of the vertical emittance is related to the cancelation of the spatial chirp and energy spread induced by the first TDS. The horizontal emittance is not affected at all and the small projected emittance growth (6 %) in the vertical plane at the minimum is due to the residual coupling generated by the system and described by Eq. (18). Nevertheless, as shown later, even in the case with CSR effects, the horizontal

slice emittance stays unaffected at all and the vertical slice emittance exhibits only deviations in the head and tail.

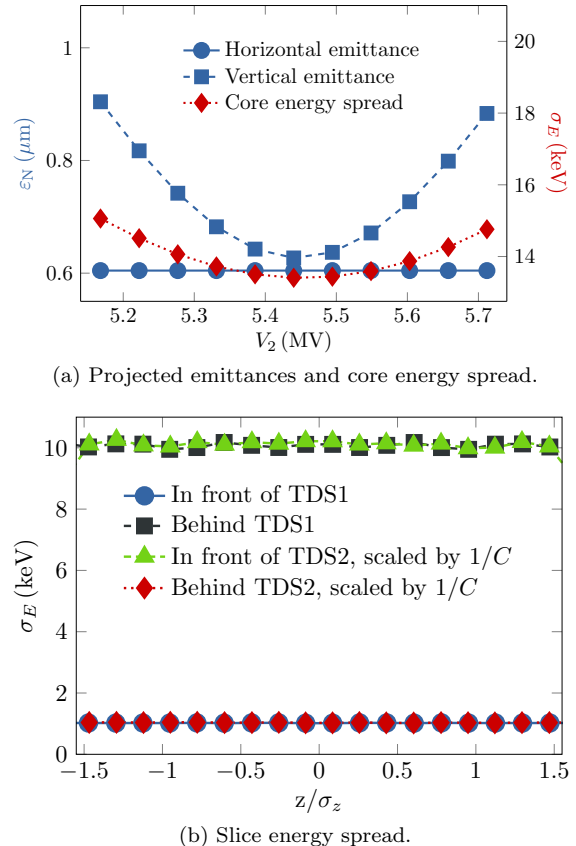
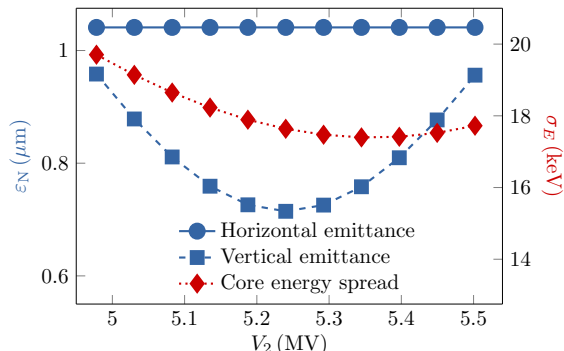


FIG. 4: Simulations without CSR effects on the impact of the reversible heater system on projected emittances, core energy spread, and slice energy spread : (a) Projected emittances (normalized) and core energy spread, and (b) slice energy spread for  $V_2$  at minimum emittance (see Fig. 4(a)). The longitudinal coordinate is normalized to the bunch length.

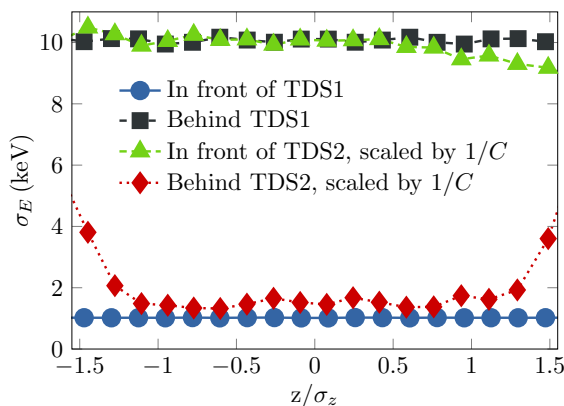
#### A. Impact of coherent synchrotron radiation

The previous results undergo small modifications when including CSR effects which is shown in Fig. 5. The voltage of the second TDS for minimum projected emittance in the vertical is shifted by about 0.2 MV to lower values which is due the additional energy chirp induced by CSR. In comparison to the case without any CSR effects (cf. Fig. 4), the projected emittance in the vertical plane is slightly increased and the slice energy spread is not perfectly canceled in the head and tail. The slice energy spread in the core part of the bunch is also slightly increased to 17.5 keV (instead of 13.5 keV in the absence of CSR). The projected emittance in the horizontal is about 1.7 larger which is independent of the reversible beam heater operation. This horizontal emittance growth can further be reduced by minimizing the horizontal beta

function in the last dipole of the chicane where the bunch length becomes the shortest. This optimization is independent of the relevant motion in the vertical and does not affect the results of the reversible heater system. Albeit the fact that the projected emittances are



(a) Projected emittances and core energy spread.



(b) Slice energy spread.

FIG. 5: Simulation on the impact of the reversible beam heater system on projected emittances, core energy spread, and slice energy spread: (a) Projected emittances (normalized) and core energy spread, and (b) slice energy spread for  $V_2$  at minimum emittance (see Fig. 5(a)). CSR effects are included by means of the 1-dimensional model in *elegant* [34].

increased, the horizontal slice emittance stays unaffected and the vertical slice emittance exhibits only deviations in the head and tail due to CSR effects as shown in Fig. 6. Thus, the core emittances are well preserved. We note that vertically streaked bunches in the bunch compressor chicane may change the impact of CSR effects but require a 3-dimensional “point-to-point” tracking which is not available neither in *elegant* nor in *CSRtrack* [36], and is beyond the scope of this paper.

#### IV. MICROBUNCHING GAIN SUPPRESSION

The principle of the microbunching gain suppression with the reversible beam heater system will be shown by an analytical treatment following Ref. [9] and using the matrix in Eq. (17). Then, we show the feasibility of the

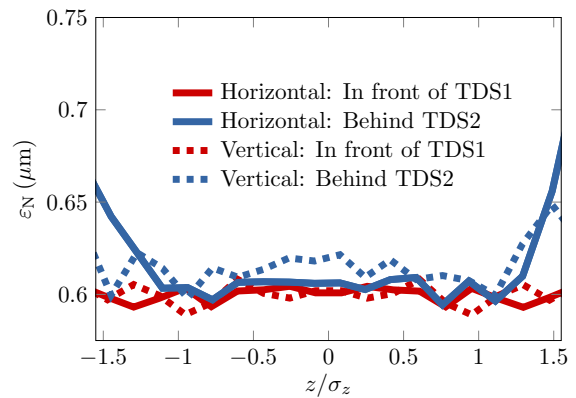


FIG. 6: Simulation of the slice emittance for both the vertical and horizontal in front of the first and behind the second TDS. CSR effects are included.

heater system to suppress microbunching instabilities by means of particle tracking simulations with initial density and energy modulations.

#### A. Analytical calculations

Although no residual energy spread is generated using the reversible beam heater system, one can see that density modulation can be suppressed by the  $z - y$  coupling term in Eq. (17). Using the vector notation  $(y_i, y'_i, z_i, \delta_i)$  for particles in the first linac, the longitudinal position behind the second TDS is

$$z_f = K_1 R_{56} y_i + (1 + h R_{56}) z_i + R_{56} \delta_i. \quad (19)$$

Suppose that  $\delta_i = \delta_0 + \delta_m$ , where  $\delta_0$  is the uncorrelated relative energy deviation, and  $\delta_m(z_i)$  is the relative energy modulation accumulated before and in the first linac (Linac1). Following Ref. [9], the initial energy modulation at the wavenumber  $k_i$  is converted into additional density modulation at a compressed wavenumber  $k_f$ . For a 4-dimensional (4-D) distribution function  $F(y_f, y'_f, z_f, \delta_f)$ , the bunching factor is given by

$$\begin{aligned} b_f(k_f) &= \int dy_f dy'_f dz_f d\delta_f e^{-ik_f z_f} F(y_f, y'_f, z_f, \delta_f) \\ &= \int dy_i dy'_i dz_i d\delta_0 e^{-ik_f K_1 R_{56} y_i - ik_f (1 + h R_{56}) z_i} \\ &\quad e^{-ik_f R_{56} (\delta_0 + \delta_m(z_i))} F_0(y_i, y'_i, z_i, \delta_0), \end{aligned} \quad (20)$$

where  $F_0(y_i, y'_i, z_i, \delta_0)$  is the initial 4-D distribution. If the induced energy modulation is small such that  $|k_f R_{56} \delta_m| \ll 1$ , we expand the exponent of Eq. (20) up to the first order in  $\delta_m$  to obtain

$$\begin{aligned} b_f(k_f) &\approx b_0(k_i) - ik_f R_{56} \int dz_i \delta_m(z_i) e^{-ik_i z_i} \\ &\quad \times \int dy_i d\delta_0 e^{-ik_f K_1 R_{56} y_i - ik_f R_{56} \delta_0} U(y_i) V(\delta_0), \end{aligned} \quad (21)$$

where  $k_f = Ck_i$ ,  $C = 1/(1 + hR_{56})$ ,  $U(y_i)$  describes the transverse profile, and  $V(\delta_0)$  is the initial energy distribution. For both Gaussian profiles, we have

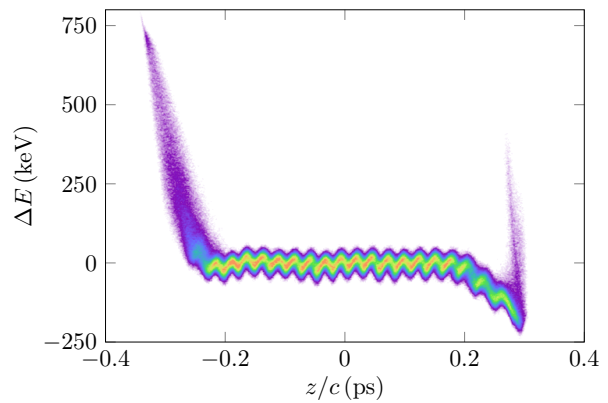
$$b_f(k_f) = b_0(k_i) - ik_f R_{56} \delta_m(k_i) \exp \left[ -(k_f^2 R_{56}^2 K_1^2 \sigma_{y1}^2 / 2) \right] \\ \times \exp \left[ -(k_f^2 R_{56}^2 \sigma_{\delta 0}^2 / 2) \right]. \quad (22)$$

Here we denote the Fourier transform of  $\delta_m(z_i)$  as  $\delta_m(k_i)$ , which is the accumulated relative energy modulation at the wavenumber  $k_i$  in the first linac due to longitudinal space charge and other collective effects.  $\sigma_{\delta 0}$  is the initial slice energy spread, and  $\sigma_{y1}$  is the vertical beam size in the first TDS. We see that  $K_1 \sigma_{y1}$  acts like effective energy spread for microbunching gain suppression.

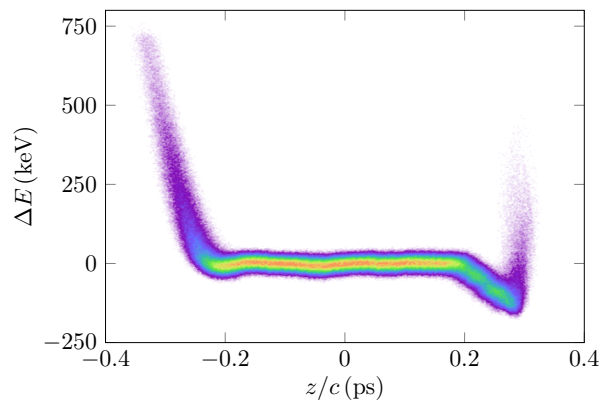
## B. Numerical simulations

Suppression of microbunching instabilities will be demonstrated by using both a pure initial density modulation with 5% amplitude and 100  $\mu\text{m}$  modulation wavelength ( $\lambda_m$ ), and a pure initial energy modulation with 3 keV peak amplitude and  $\lambda_m = 50 \mu\text{m}$ . Whereas the case with initial energy modulation is immediately consistent with the previous analytical treatment and describes the longitudinal space charge driven microbunching instability [7], the initial density modulations need to be converted into energy modulations by longitudinal CSR-impedance which expresses the consistency and describes the CSR-driven microbunching instability [6]. The simulations were performed using *elegant* and  $1 \times 10^6$  particles. Figure 7 shows the longitudinal phase space behind the second TDS for both the reversible beam heater system switched off (Fig. 7(a)) and on (Fig. 7(b)). In the case without reversible beam heater, energy and density modulations at the compressed modulation wavelength  $\lambda_m/C$  appear, i.e., CSR-driven microbunching becomes visible. When switching the reversible beam heater on, the microbunching instability disappears and the resulting longitudinal phase space remains smooth. The reason is that the microbunches at the compressed wavelength will be smeared due to  $R_{56} K_1 \sigma_{y1}$  (cf. Eqs. (22) and (17)), and accordingly, the modulations appear as correlations in the phase spaces  $(y, z)$  and  $(y', \delta)$ . The same effect of microbunching suppression is given for initial energy modulations as shown in Fig. 8. The effect of the microbunching instability is even stronger compared to the simulations case with initial density modulations, but the performance of the reversible heater system is the same with a smooth residual longitudinal phase space when the heater is switched on in Fig. 8(b). The general shape of the longitudinal phase space is similar to the case in Fig. 7, so that a different axes scale was used for the sake of clarity.

Figures 7 and 8 are obtained for a bunch compressor system as shown in Fig. 1. The bunch will be further accelerated and transported throughout the rest of the accelerator to reach the final beam energy and peak



(a) Behind TDS2: Heater system off.



(b) Behind TDS2: Heater system on.

FIG. 7: Simulation on suppression of microbunching instabilities due to an initial density modulation, i.e., CSR-driven microbunching. The entire longitudinal phase space is shown.

current in order to drive a X-ray FEL (not studied in this paper). A microbunched beam as illustrated in Figures 7(a) and 8(a), i.e., when the reversible beam heater system is switched off, will accumulate additional energy and density modulations, leading to unacceptable longitudinal phase space properties for an X-ray FEL such as a large slice energy spread.

## V. PRACTICAL CONSIDERATIONS

The previous sections covered the principle of reversible electron beam heating and microbunching gain suppression by means of analytical calculations and numerical simulations. In real accelerators and machines we also have to deal with imperfection, jitter and drifts of various parameters, and accordingly supplementary study with respect to sensitivity on jitter sources and tolerances has to be performed. In the following, we discuss the impact of beam and rf jitter on the heater system, and also point out the inherent possibility of longitudinal phase space diagnostics and monitoring.

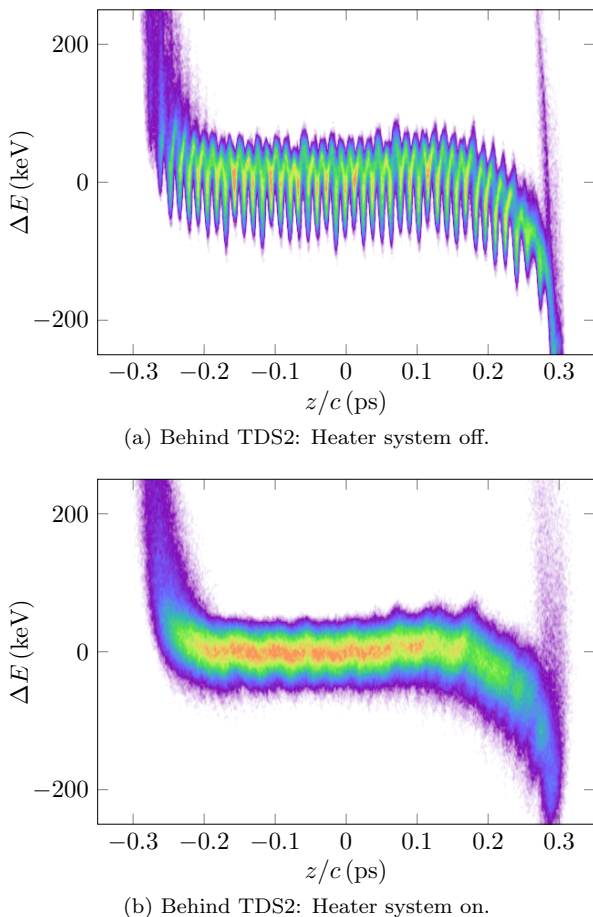


FIG. 8: Simulation on suppression of microbunching instabilities due to an initial energy modulation, i.e., longitudinal space charge driven microbunching. For the sake of clarity, only the core of the longitudinal phase space is shown.

### A. Jitter and tolerances

The impact of beam and rf jitter can effectively be discussed using the Eqs. (2) and (17), where in the latter case, the condition in Eq. (15) is already fulfilled. Deviations from this conditions can appear from jitter of the individual peak deflection voltages  $V_1$  and  $V_2$  of the TDSs, and lead to growth of the projected vertical emittance as shown in Fig. 5(a), where the voltage of the second TDS is varied. Even in the case of a large voltage jitter of 1%, the vertical projected emittance growth will be less than 2%. In the case of acceleration between the first and second TDS, also energy jitter due to this intermediate acceleration leads to deviation of the condition in Eq. (15), and is similar or smaller than TDS voltage jitter. The choice of superconducting accelerator technology even provide much better rf stability [37, 38]. Pure arrival time jitter has no impact as long as the condition in Eq. (15), which describes the coupling between  $y'$  and  $t = z/c$ , is fulfilled. In the case of deviations, e.g., due to voltage jitter which will be on the percent-level,

and typical arrival time jitter well below 100fs like at LCLS [3] or FLASH [38], this is negligible. The most critical jitter sources arise from energy jitter upstream of the bunch compressor chicane and rf phase jitter in the TDSs. The momentum compaction factor translates energy jitter into arrival time jitter, which leads to centroid kicks in the second TDS. The same effect of additional centroid kicks is generated by rf phase jitter in the TDSs. In order to have small impact of centroid kicks on the remaining beam transport, we demand  $\Delta y' \ll \sigma_{y'}$  directly behind the second TDS, with  $\Delta y'$  being the induced centroid kick and  $\sigma_{y'}$  the beam divergence. The relevant total centroid kick will be

$$\begin{aligned} \Delta y' &= \sqrt{\left(K_2 R_{56} \frac{\sigma_E}{E}\right)^2 + \left(K_2 \frac{c}{\omega} \sigma_{\varphi_2}\right)^2 + \left(\frac{K_1}{a} \frac{c}{\omega} \sigma_{\varphi_1}\right)^2} \\ &= \sqrt{\left(K_2 R_{56} \frac{\sigma_E}{E}\right)^2 + \left(K_2 \frac{c}{\omega}\right)^2 \left(\sigma_{\varphi_2}^2 + \frac{1}{C^2} \sigma_{\varphi_1}^2\right)} \\ &\approx \sqrt{\left(K_2 R_{56} \frac{\sigma_E}{E}\right)^2 + \left(K_2 \frac{c}{\omega}\right)^2 \sigma_{\varphi_2}^2} \end{aligned} \quad (23)$$

with the energy jitter  $\sigma_E/E$ , the rf phase jitter  $\sigma_{\varphi_{1,2}}$ , the magnification factor  $a$  from the first to the second TDS (see Eq. (13)), and using Eq. (15) with the compression factor  $C = (1 + hR_{56})^{-1}$ . We see that the kick due to rf phase jitter in the first TDS scales with  $C^{-2}$  and can be neglected compared to the kick induced by the second TDS when we assume the same amount of rf phase jitter in both TDSs. The condition for trajectory stability  $\Delta y'_2 \ll \sigma_{y'_2} = \sqrt{\epsilon_{y_2}(1 + \alpha_{y_2}^2)}/\beta_{y_2}$ , with the geometrical emittance  $\epsilon_{y_2}$  and  $\alpha_{y_2} = -\beta'_{y_2}(s)/2$ , can be restated as (omitting the index  $y$ )

$$\begin{aligned} \sqrt{\left(R_{56} \frac{\sigma_E}{E}\right)^2 + \left(\frac{c}{\omega} \sigma_{\varphi_2}\right)^2} &\ll \frac{\epsilon_2}{K_2 \sqrt{\beta_2 \epsilon_2}} \sqrt{1 + \alpha_2^2} \\ &= \frac{\epsilon_2}{C \Delta \sigma_\delta} \sqrt{1 + \alpha_2^2}, \end{aligned} \quad (24)$$

where  $\Delta \sigma_\delta$  is the additional relative energy spread induced by the first TDS for suppression of microbunching instabilities. We see that only the Twiss parameter  $\alpha_2$  leave some room for independent optimization, whereas a smaller  $R_{56}$  would need to be compensated with a larger energy chirp  $h$  to keep the required compression  $C$  and lead to a corresponding higher energy jitter.

For the example parameters discussed throughout this paper, the stability condition yields acceptable pure relative energy jitter of  $\sigma_E/E \ll 3.8 \cdot 10^{-5}$  or pure rf phase jitter of  $\sigma_{\varphi_2} \ll 0.025^\circ$ . A combination of both will obviously tighten the acceptable jitter. This level of stability is difficult to achieve in normal conducting linacs with single bunch operation, but is realistic with superconducting accelerator technology like at FLASH, where many bunches can be accelerated in a long rf pulse, i.e., in a bunch train. Currently, several rf feed-forward and feedback controls are able to stabilize the

bunches at FLASH to  $\sigma_E/E = 3.0 \cdot 10^{-5}$  at 150 MeV and  $\sigma_\varphi = 0.007^\circ$  [37, 39], and further improvements towards  $\sigma_E/E \leq 1.0 \cdot 10^{-5}$  are planned using a fast normal conducting cavity in front of the bunch compressors [37, 38]. With perfect scaling of jitter from independent rf stations that adds uncorrelated, we would expect an improvement of  $\sqrt{150/350} \approx 0.66$  compared to the results at FLASH. Continuous-wave rf operation, as planned for NGLS [26], and a proper choice of rf working points might improve stability further.

### B. Integrated longitudinal phase space diagnostics

A practical spin-off of the reversible beam heater system is the availability of longitudinal phase space diagnostics. The vertical betatron motion of an electron passing through a TDS is described by Eq. (4) which enables a mapping from time (longitudinal coordinate) to the vertical plane, and finally a possibility to obtain temporal bunch information by means of transverse diagnostics. In a similar manner, the relative energy is mapped to the horizontal plane in the presence of horizontal momentum dispersion like in a magnetic bunch compressor chicane (e.g., Refs. [15, 16]). Both in combination make single-shot measurements of the longitudinal phase space possible. In the case of the generic layout of an reversible electron beam heater system depicted in Fig. 1, longitudinal phase space measurements are possible using the first TDS and an observation screen in the dispersive section between the second and third bending magnet. In this configuration, the longitudinal phase space in front of the bunch compressor, i.e., before the compression process takes place, can be investigated. This can be useful to observe and control longitudinal phase linearization in order to achieve and maintain uniform bunch compression (e.g., see Fig. 36 in Ref. [40]). For the accelerator optics shown in Fig. 2, the heater system related parameters in Table I, and according to the estimation formulae given in Refs. [15, 31], a relative energy resolution of  $\sim 2 \cdot 10^{-4}$  (r.m.s.) and a time resolution of  $\sim 130$  fs (r.m.s.) can be achieved, which is sufficient for uncompressed bunches coming from the injector, and can even be improved. In order to get information of the bunch length after the bunch compression, the second TDS can be used with a downstream observation screen not shown in Fig. 1. With the given parameters and assuming a vertical phase advance of about  $\pi/2$  from the TDS to a potential screen, a time resolution of  $\sim 10$  fs (r.m.s.) can be expected. Using a quadrupole in the middle of the bunch compressor chicane for generation of dispersion leakage (as shown at SACLA [41]), even longitudinal phase space measurements after bunch compression become feasible. In addition to invasive longitudinal phase space measurements of a single (or a few) bunches with an observation screen in the middle of the chicane and using the first TDS, even a fully parasitic measurement utilizing incoherent synchrotron radiation, emitted in the second or

third bunch compressor bending magnet, is possible [42]. The implication will be the possibility of nondestructive single-shot monitoring of the longitudinal phase space. At multi-bunch machines, this would result in the capability of monitoring individual bunches of a so-called bunch train when using a fast gated camera.

## VI. SUMMARY AND CONCLUSIONS

Our studies show that the reversible beam heater system proposed here can suppress microbunching instabilities and preserve the high beam brightness at the same time. Due to CSR effects, some vertical emittance degradation in the head and tail region of the bunch occurs, but the core emittances are well preserved. In the numerical demonstration, the first TDS generates about 10 keV slice energy spread similar to a laser heater, but with a more Gaussian energy distribution compared with the laser heater. The bunch compression process increases the slice energy spread to  $\sim 130$  keV, which is then reversed to  $\sim 17$  keV after the second TDS in presence of CSR effects. Without CSR effects, the slice energy spread is reversed to  $\sim 13$  keV which shows perfect cancelation. Simulations also show that initial bunching in energy and density in the beam can be smeared out during the process in the reversible beam heater system, i.e., microbunching instabilities can be suppressed. The resulting smooth beam can then propagate through the remaining accelerator without further generation of much additional energy spread and is advantageous for any kind of laser seeding manipulations and experiments. For example, this scheme will significantly loosen the required laser power for short-wavelength HHG seeding [10] and may strongly impact the design of future seeded FELs. In addition, the reversible beam heater system exhibits inherent options for diagnosis and on-line monitoring of the longitudinal phase space applicable for multi-bunch machines which is also the preferred type of accelerator for the reversible heater system due to large sensitivities on energy and rf jitter. Linear accelerators based on superconducting rf technology will be able to match the strict tolerances in order to keep centroid kicks small and achieve a sufficient trajectory stability.

### Acknowledgments

We would like to thank P. Emma, Ch. Gerth, A. Lumpkin, H. Schlarb, and J. Thangaraj for useful discussions and suggestions. This work was supported by Department of Energy Contract No. DE-AC02-76SF00515.

### Appendix: Uniform bunch compression

Here we derive the condition for uniform compression across the entire bunch, as required by the reversible

heater scheme. The path length dependence on energy up to the second-order in energy deviation is given by

$$z_f = R_{56}\delta_i + T_{566}\delta_i^2. \quad (\text{A.1})$$

The effective (energy-dependent)  $R_{56}^{eff}$  is

$$R_{56}^{eff} = \frac{dz_f}{d\delta_i} = R_{56} + 2T_{566}\delta_i. \quad (\text{A.2})$$

If we now introduce a quadratic chirp in the electron beam, i.e.,  $\delta_i = hz_i + qz_i^2$ , the effective linear chirp is

$$h^{eff} = \frac{d\delta_i}{dz_i} = h + 2qz_i. \quad (\text{A.3})$$

Thus, the local compression factor is determined by the product

$$\begin{aligned} h^{eff}R_{56}^{eff} &= (h + 2qz_i)(R_{56} + 2T_{566}\delta_i) \\ &\approx hR_{56} + 2qR_{56}z_i + 2T_{566}h^2z_i. \end{aligned} \quad (\text{A.4})$$

Higher-order terms are ignored in the last equality. The coefficient of the quadratic chirp can be chosen as

$$q = -\frac{T_{566}}{R_{56}}h^2. \quad (\text{A.5})$$

For a simple 4-dipole chicane,  $T_{566} = -3R_{56}/2$ , and hence  $q = 3h^2/2$ . In order to have uniform compression across the entire bunch (i.e., the local compression

factor must be independent of  $z_i$ ), this quadratic chirp can be introduced by the higher-harmonic rf linearizer as commonly found in X-ray FEL designs (see Fig. 1). Figure 9 shows the applied uniform bunch compression

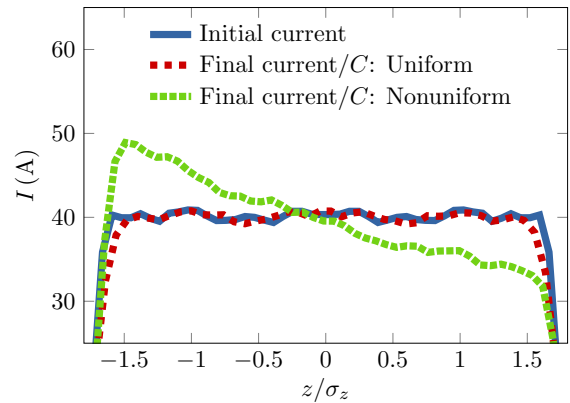


FIG. 9: Initial and final longitudinal bunch profiles (final currents scaled by the inverse compression), and applied uniform compression used throughout the simulations in this paper.

by means of longitudinal bunch profiles in front (initial current) and behind (final current) the magnetic bunch compressor chicane used throughout the simulations in this paper. Nonuniform bunch compression is related to the case with a perfect linear energy chirp in front of the bunch compressor chicane that results in a non-constant current which is due to the higher-order term  $T_{566}$ .

- 
- [1] S. Jamison, *Nature Photonics* **4**, 589 - 591 (2010).  
[2] W. Ackermann *et al.*, *Nature Photonics* **1**, 336 - 342 (2007).  
[3] P. Emma *et al.*, *Nature Photonics* **4**, 641 - 647 (2010).  
[4] D. Pile, *Nature Photonics* **5**, 456 - 457 (2011).  
[5] E. L. Saldin, E. A. Schneidmiller, and M.V. Yurkov, *Nucl. Instrum. Methods Phys. Res., Sect. A* **398**, 373 (1997).  
[6] M. Borland *et al.*, *Nucl. Instrum. Methods Phys. Res., Sect. A* **483**, 268 (2002).  
[7] E.L. Saldin, E.A. Schneidmiller, and M.V. Yurkov, *Nucl. Instrum. Methods Phys. Res., Sect. A* **528**, 355 (2004).  
[8] Z. Huang, M. Borland, P. Emma, J. Wu, C. Limborg, G. Stupakov, and J. Welch, *Phys. Rev. ST Accel. Beams* **7**, 074401 (2004).  
[9] Z. Huang *et al.*, *Phys. Rev. ST Accel. Beams* **13**, 020703 (2010).  
[10] D. J. Dunning *et al.*, *Proceedings of the 1st International Particle Accelerator Conference, Kyoto, Japan, 2010*, TUPE049.  
[11] M. Cornacchia, S. Di Mitri, G. Penco, and A. Zholents, *Phys. Rev. ST Accel. Beams* **9**, 120701 (2006).  
[12] Y. Ding, P. Emma, Z. Huang, and V. Kumar, *Phys. Rev. ST Accel. Beams* **9**, 070702 (2006).  
[13] O. Altenmueller, R. Larsen, and G. Loew, *Rev. Sci. Instrum.* **35**, 438 (1964).  
[14] P. Emma, J. Frisch, and P. Krejcik, *Technical Report No. LCLS-TN-00-12*, 2000.  
[15] M. Röhrs, Ch. Gerth, H. Schlarb, B. Schmidt, and P. Schmüser, *Phys. Rev. ST Accel. Beams* **12**, 050704 (2009).  
[16] D. Filippetto *et al.*, *Phys. Rev. ST Accel. Beams* **14**, 092804 (2011).  
[17] Y. Ding, C. Behrens, P. Emma, J. Frisch, Z. Huang, H. Loos, P. Krejcik, and M-H. Wang, *Phys. Rev. ST Accel. Beams*, in press.  
[18] A. Zholents, P. Heimann, M. Zolotarev, and J. Byrd, *Nucl. Instrum. Methods Phys. Res., Sect. A* **425**, 385 (1999).  
[19] M. Cornacchia and P. Emma, *Phys. Rev. ST Accel. Beams* **5**, 084001 (2002).  
[20] P. Emma, Z. Huang, K.-J. Kim, and P. Piot, *Phys. Rev. ST Accel. Beams* **9**, 100702 (2006).  
[21] D. Xiang and Y. Ding, *Phys. Rev. ST Accel. Beams* **13**, 094001 (2010).  
[22] P. Piot, Y.-E Sun, J. G. Power, and M. Rihaoui, *Phys. Rev. ST Accel. Beams* **14**, 022801 (2011).  
[23] D. Xiang and A. Chao, *Phys. Rev. ST Accel. Beams* **14**, 114001 (2011).  
[24] D. Xiang *et al.*, *Phys. Rev. Lett.* **105**, 114801 (2010).  
[25] D. Xiang *et al.*, *Proceedings of the 33rd International*

- Free Electron Laser Conference, Shanghai, China, 2011, WEOB4.
- [26] J. Corlett *et al.*, Proceedings of the 24th Particle Accelerator Conference, New York, USA, 2011, TUOCS5.
- [27] M. Venturini and A. Zholents, Nucl. Instrum. Methods Phys. Res., Sect. A **593**, 53 (2008).
- [28] H. Edwards, C. Behrens, and E. Harms, Proceedings of the 25th International Linear Accelerator Conference, Tsukuba, Japan, 2010, MO304.
- [29] W. Panofsky and W. Wenzel, Rev. Sci. Instrum. **27**, 967 (1956).
- [30] S. Korepanov, M. Krasilnikov, F. Stephan, D. Alesini, and L. Ficcadenti, Proceedings of the 8th European Workshop on Beam Diagnostics and Instrumentation for Particle Accelerators, Venice, Italy, 2007, TUPB32.
- [31] C. Behrens and Ch. Gerth, Proceedings of the 9th European Workshop on Beam Diagnostics and Instrumentation for Particle Accelerators, Basel, Switzerland, 2009, TUPB44.
- [32] C. Behrens and Ch. Gerth, Proceedings of the 10th European Workshop on Beam Diagnostics and Instrumentation for Particle Accelerators, Hamburg, Germany, 2011, TUPD31.
- [33] P. Emma (private communication).
- [34] M. Borland, ANL/APS Report No. LS-287, 2000.
- [35] M. Venturini *et al.*, Proceedings of the 24th Particle Accelerator Conference, New York, USA, 2011, THP180.
- [36] M. Dohlus and T. Limberg, Proceedings of the 26th International Free Electron Laser Conference, Trieste, Italy, 2004, MOCOS05.
- [37] H. Schlarb (private communication).
- [38] C. Schmidt *et al.*, Proceedings of the 33rd International Free Electron Laser Conference, Shanghai, China, 2011, THPA26.
- [39] S. Pfeiffer *et al.*, LLRF-2011 workshop, Hamburg, Germany, 2011, “Feedback Strategies for longitudinal Beam Stabilization”.
- [40] R. Akre *et al.*, Phys. Rev. ST Accel. Beams **11**, 030703 (2008).
- [41] Y. Otake (private communication).
- [42] Ch. Gerth, Proceedings of the 8th European Workshop on Beam Diagnostics and Instrumentation for Particle Accelerators, Venice, Italy, 2007, TUPC03.